

Direct Silicon-nitrogen Bonded Host Materials with Enhanced σ - π Conjugation for Blue Phosphorescent Organic Light-emitting Diodes

Huanhuan Li^{a,b}, Lijia Xu^a, Yuting Tang^a, Ye Tao^a, Shen Xu^a, Chao Zheng^{*a}, Guichuan Xing^b, Xinhui Zhou^a, Wei Huang^{*b}, Runfeng Chen^{*a}

^aKey Laboratory for Organic Electronics and Information Displays & Institute of Advanced Materials (IAM), National Synergetic Innovation Center for Advanced Materials (SICAM), Nanjing University of Posts & Telecommunications, 9 Wenyuan Road, Nanjing 210023, P.R. China

E-mail: iamrfchen@njupt.edu.cn; wei-huang@njupt.edu.cn. Fax: +86 25 8586 6396. Tel: +86 25 8586 6396

^bKey Laboratory of Flexible Electronics (KLOFE) & Institute of Advanced Materials (IAM), National Synergetic Innovation Center for Advanced Materials (SICAM), Nanjing Tech University (Nanjing Tech), 30 South Puzhu Road, Nanjing 211816, P.R. China.

Content

1. Synthesis and characterization	2
2. Single crystal analysis.....	9
3. Features of N-Si bond	11
4. Atomic force microscopy.....	12
5. Thermal properties	13
6. Optical properties.....	13
7. Electrochemical properties.....	14
8. DFT calculations.....	15
9. Charge mobility	16
10. Device fabrications and measurements	17

1. Synthesis and characterization

Materials: The manipulations involving air-sensitive reagents were performed in an atmosphere of dry N₂. The chemicals and solvents, unless otherwise specified, were purchased from Aladdin, Aldrich or Acros, and used without further purification. Tetrahydrofuran (THF) was dried and purified in a standard procedure.

Characteristic Methods: ¹H and ¹³C-nuclear magnetic resonance (NMR) spectra were recorded on a Bruker Ultra Shield Plus 400 MHz instrument using *d*-CDCl₃ as the solvent and tetramethylsilane (TMS) as the internal standard. The quoted chemical shifts are in *ppm* and the *J* values are expressed in Hz. The splitting patterns have been designed as follows: s (singlet), d (doublet), t (triplet), dd (doublet of doublets), and m (multiplet). The MALDI-TOF-MS was performed on a Bruker Daltonics flex Analysis. High resolution mass spectroscopy (HRMS) were recorded on a LCT Premier XE (Waters) mass spectrometer.

The synthesis of 9-(triphenylsilyl)-9H-carbazole (CzSi)

Carbazole (2.0 g, 12 mmol) dissolved in anhydrous THF (40 mL) under nitrogen protection was cooled to 0°C by an ice/water bath. *n*-Butyl lithium (8.3 mL, 13.2 mmol, 1.6 M in hexane) was then added dropwise to give a bright yellow solution, which was then thickened to form a slurry. After the lithiation reaction of carbazole at 0°C for 1 h, a solution of chlorotriphenylsilane (4.3 g, 14.4 mmol) in THF was added into. The reaction mixture was stirred at 0°C for 1 h, and then allowed warm to room temperature and stir overnight. The reaction was quenched with water (50 mL) and extracted with dichloromethane (CH₂Cl₂) for three times (3×200 mL). The organic phase was separated, collected, dried, and concentrated under reduced pressure. The crude solid product was purified further by flash column chromatography on silica gel (300-400 mesh). Yield: 4.3 g of white solid (85%). ¹H NMR (400 MHz, CDCl₃, *ppm*): δ 6.70 (d, *J*=8.4 Hz, 2H), 7.02 (t, *J*=8 Hz, 2H), 7.19 (t, *J*=7.2 Hz, 2H), 7.41 (t, *J*=7.2 Hz, 6H), 7.51 (m, 3H), 7.67 (d, *J*=7.2 Hz, 6H), 8.10 (d, *J*=7.2 Hz, 2H); ¹³C NMR (100 MHz, CDCl₃, *ppm*): δ 114.92, 119.69, 119.97, 125.17, 126.51, 128.40, 130.65, 132.47, 136.11, 144.74. MALDI-TOF: *m/z* calcd for C₃₀H₂₃NSi: 425.160 [M]; found: 425.429. HRMS (EI): *m/z* calcd: 425.1678 [M+H]⁺; found: 426.1681.

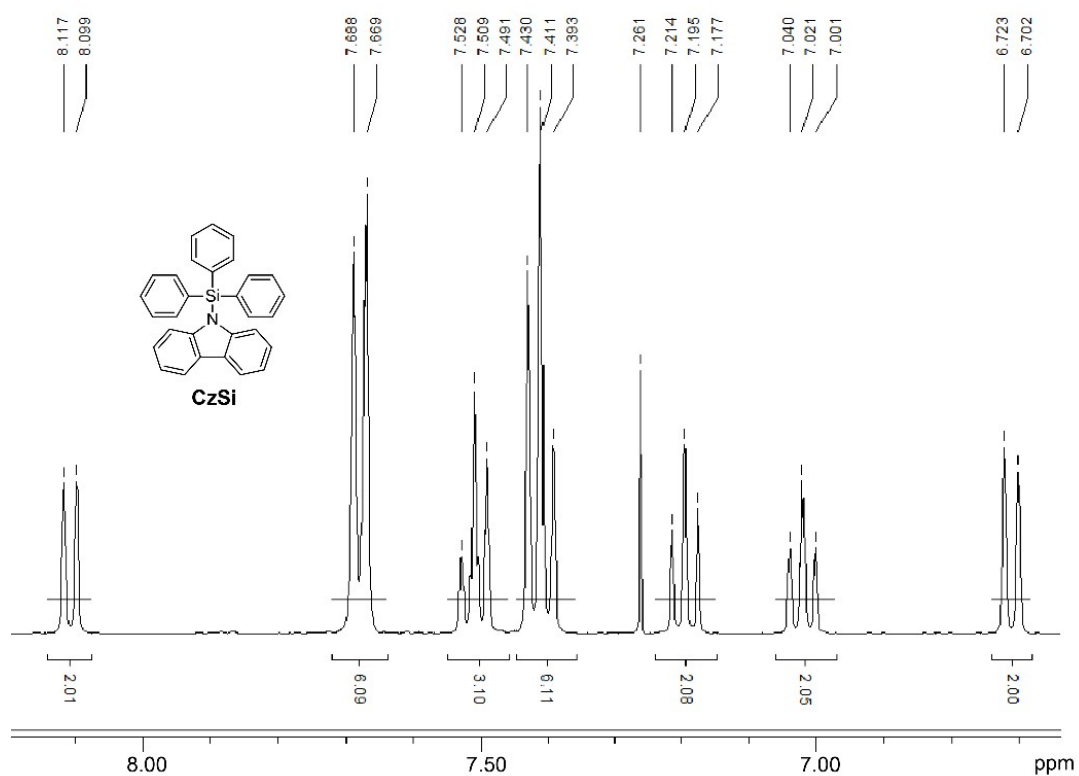


Figure S1. ^1H NMR spectrum of 9-(triphenylsilyl)-9H-carbazole (CzSi).

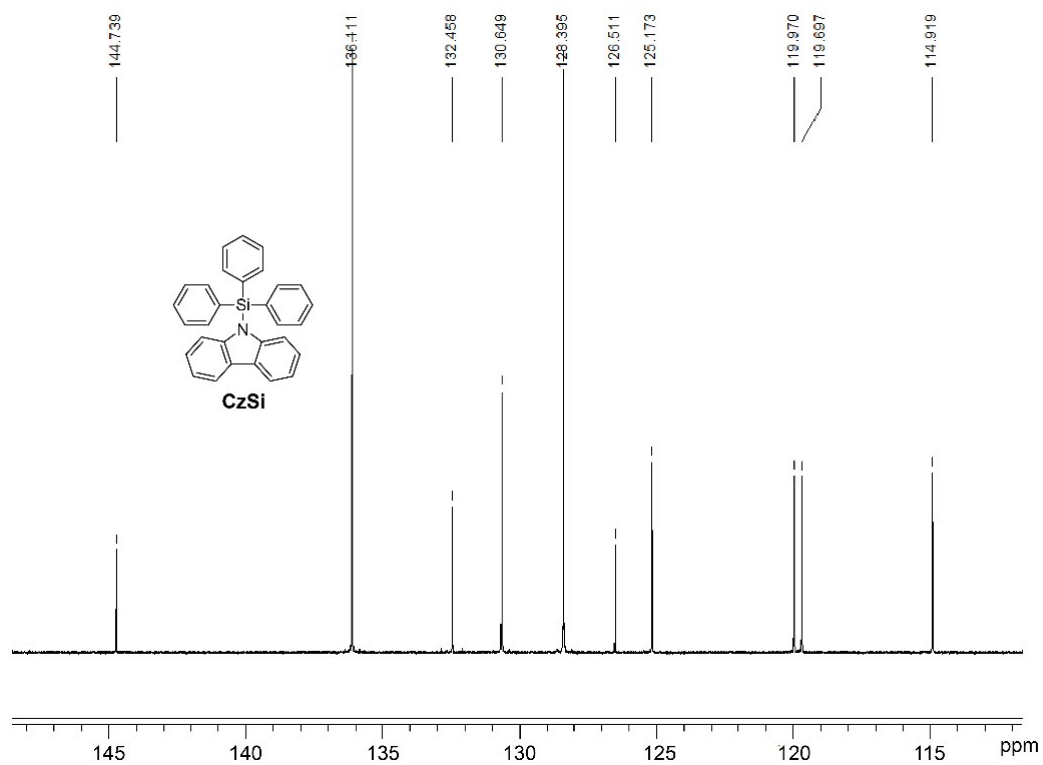


Figure S2. ^{13}C NMR spectrum of 9-(triphenylsilyl)-9H-carbazole (CzSi).

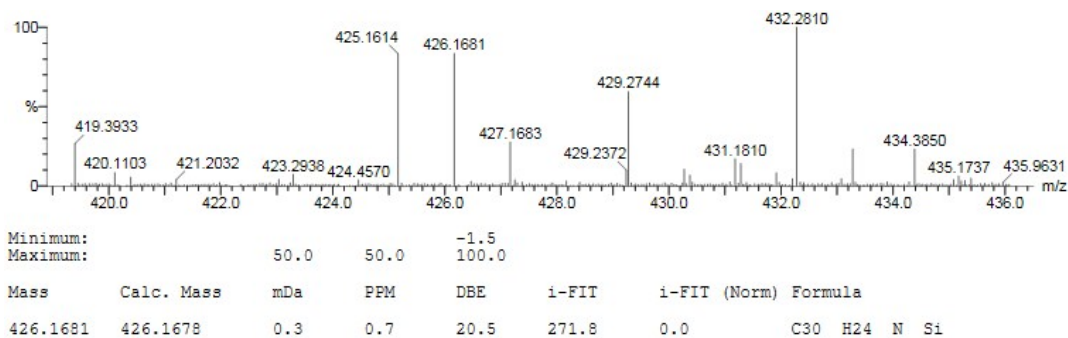


Figure S3. HRMS spectrum of 9-(triphenylsilyl)-9H-carbazole (**CzSi**).

The synthesis of di(9H-carbazol-9-yl)diphenylsilane (**DCzSi**)

DCzSi was synthesized and purified in a similarly way of **CzSi** by using 2.0 g carbazole (12 mmol), 8.3 mL *n*-butyl lithium (13.2 mmol, 1.6 M in hexane) and 1.0 mL dichlorodiphenylsilane (5 mmol). Yield: 2.0 g of white solid (78%). ¹H NMR (400 MHz, CDCl₃, ppm): δ 6.78 (d, *J*=8.4 Hz, 4H), 6.96 (t, *J*=8.4 Hz, 4H), 7.19 (t, *J*=7.2 Hz, 4H), 7.37 (t, *J*=8 Hz, 4H), 7.52 (t, *J*=9.6 Hz, 2H), 7.73 (d, *J*=9.2 Hz, 4H), 8.08 (d, *J*=8.4 Hz, 4H); ¹³C NMR (100 MHz, CDCl₃, ppm): δ 114.86, 119.79, 120.73, 125.71, 126.85, 128.59, 131.21, 131.51, 136.40, 143.88. MALDI-TOF: *m/z* calcd for C₃₆H₂₆N₂Si: 514.186 [M]; found: 514.690. HRMS (EI): *m/z* calcd: 515.1944 [M+H]⁺; found: 515.1946.

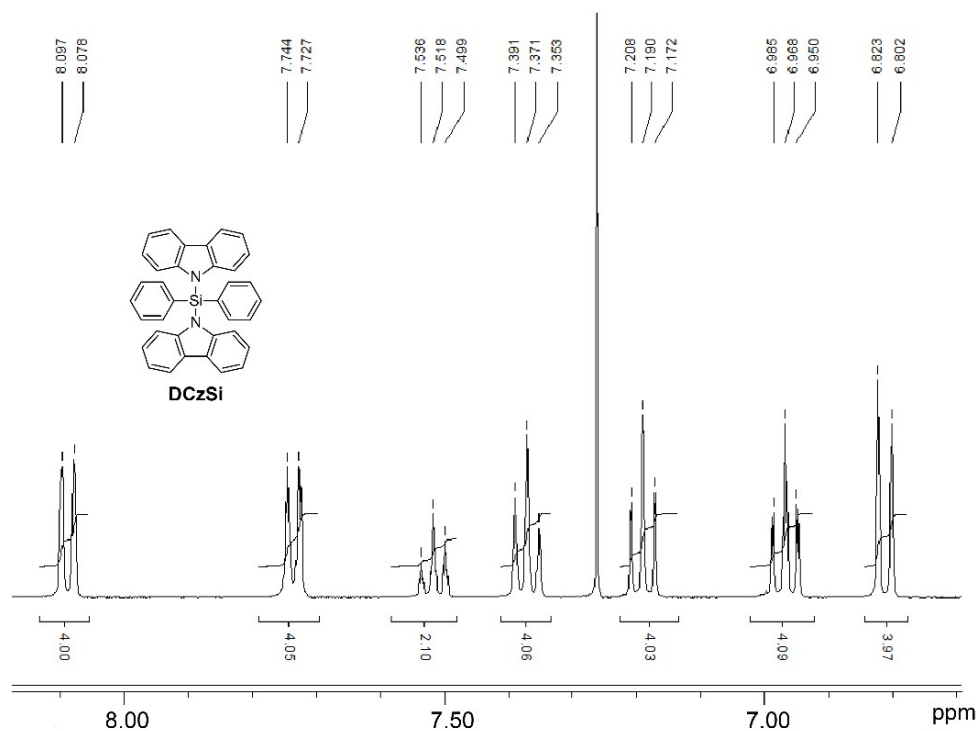


Figure S4. ¹H NMR spectrum of di(9H-carbazol-9-yl)diphenylsilane (**DCzSi**).

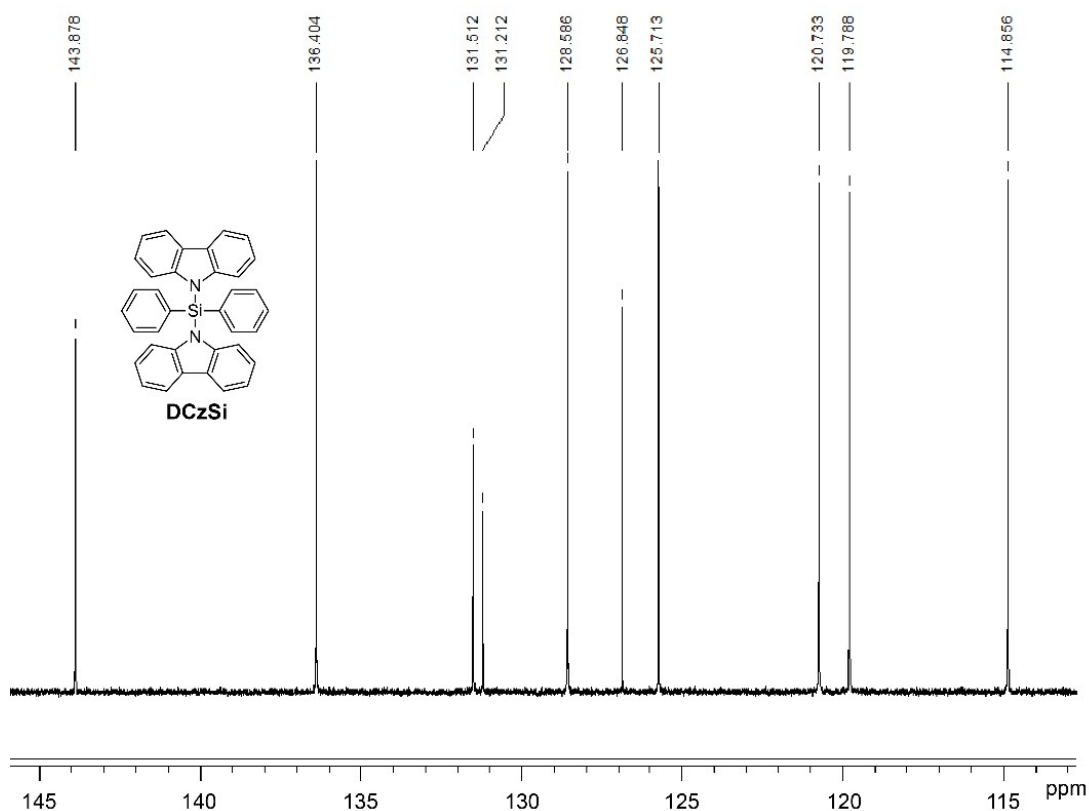


Figure S5. ^{13}C NMR spectrum of di(9H-carbazol-9-yl)diphenylsilane (DCzSi).

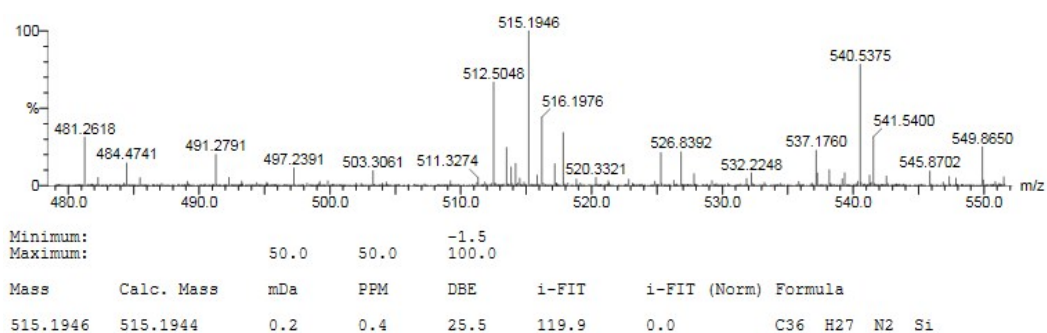


Figure S6. HRMS spectrum of di(9H-carbazol-9-yl)diphenylsilane (DCzSi).

The synthesis of 3,6-di-*tert*-butyl-9-(triphenylsilyl)-9H-carbazole (BuCzSi)

BuCzSi was also prepared following the standard synthetic route of CzSi using 3,6-di-*tert*-butyl-9H-carbazole (3.4 g, 12 mmol), *n*-butyllithium (8.3 mL, 13.2 mmol, 1.6 M in hexane) and chlorotriphenylsilane (4.3 g, 14.4 mmol). Yield: 5.2 g of white solid (90%). ^1H NMR (400 MHz, CDCl_3 , ppm): δ 1.41 (s, 18H), δ 6.57 (d, $J=8.8$ Hz, 2H), 7.02 (d, $J=8.8$ Hz, 2H), 7.40 (m, 6H), 7.50 (t, $J=7.2$ Hz, 3H), 7.66 (t, $J=7.6$ Hz, 6H), 8.09 (s, 2H); ^{13}C NMR (100 MHz, CDCl_3 , ppm): δ 31.93,

34.56, 114.16, 115.55, 122.93, 126.39, 128.31, 130.51, 132.75, 136.17, 142.63, 143.11. MALDI-TOF: m/z calcd for $C_{36}H_{26}N_2Si$: 537.808 [M]; found: 537.946. HRMS (EI): m/z calcd: 538.2930 [M+H]⁺; found: 538.2925.

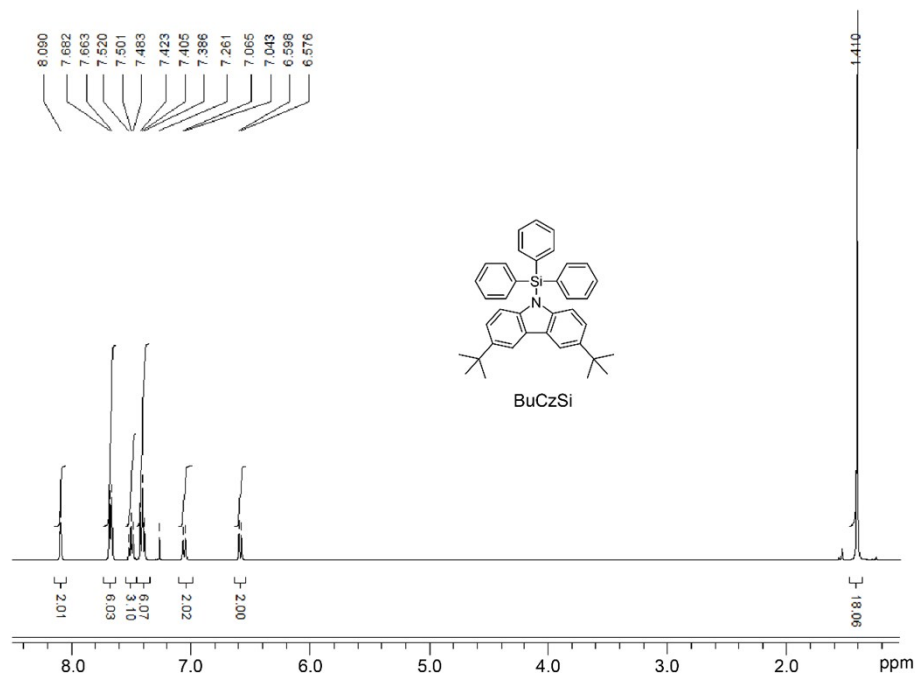


Figure S7. ¹H NMR spectrum of 3,6-di-*tert*-butyl-9-(triphenylsilyl)-9H-carbazole (**BuCzSi**).

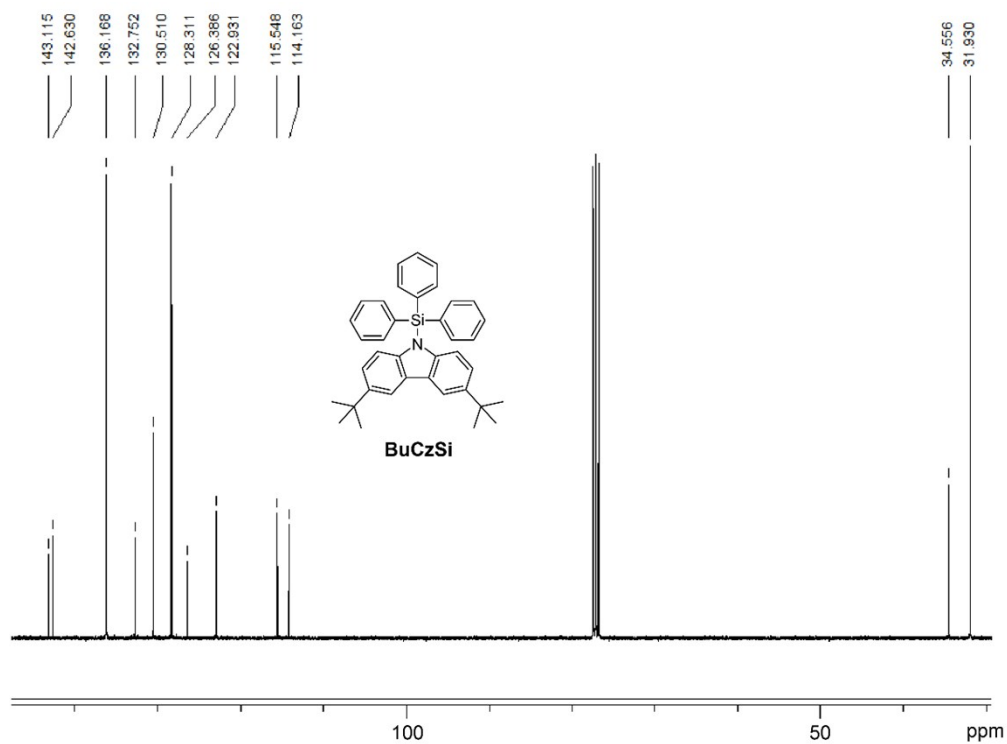


Figure S8. ¹³C NMR spectrum of 3,6-di-*tert*-butyl-9-(triphenylsilyl)-9H-carbazole (**BuCzSi**).

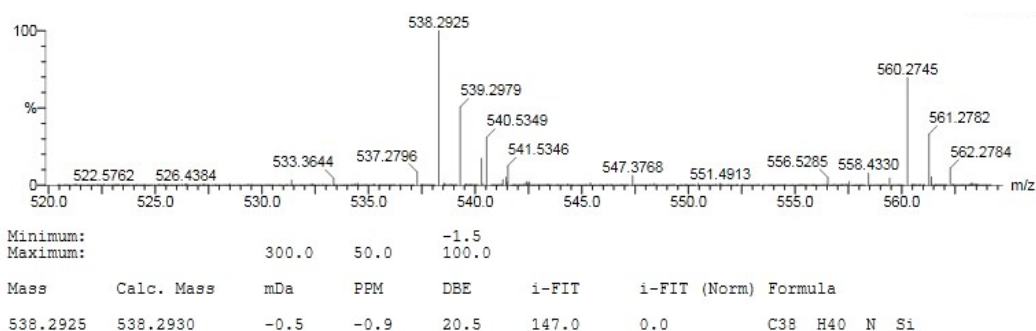


Figure S9. HRMS spectrum of 3,6-di-*tert*-butyl-9-(triphenylsilyl)-9H-carbazole (**BuCzSi**).

The synthesis of bis(3,6-di-*tert*-butyl-9H-carbazol-9-yl)diphenylsilane (**DBuCzSi**)

DBuCzSi was obtained in a similar way as in preparing **CzSi** using 3,6-di-*tert*-butyl-9H-carbazole (3.4 g, 12 mmol), *n*-butyllithium (8.3 mL, 13.2 mmol, 1.6 M in hexane), and dichlorodiphenylsilane (1.0 mL, 5 mmol). Yield: 3.0 g of white solid (75%). ¹H NMR (400 MHz, CDCl₃, *ppm*): δ 6.78 (d, *J*=8.4 Hz, 4H), 6.96 (t, *J*=8.4 Hz, 4H), 7.19 (t, *J*=7.2 Hz, 4H), 7.37 (t, *J*=8 Hz, 4H), 7.52 (t, *J*=9.6 Hz, 2H), 7.73 (d, *J*=9.2 Hz, 4H), 8.08 (d, *J*=8.4 Hz, 4H); ¹³C NMR (100 MHz, CDCl₃, *ppm*): δ 114.86, 119.79, 120.73, 125.71, 126.85, 128.59, 131.21, 131.51, 136.40, 143.88. MALDI-TOF: *m/z* calcd for C₃₆H₂₆N₂Si: 739.116 [M]; found: 739.219. HRMS (EI): *m/z* calcd: 761.4267 [M+Na]⁺; found: 761.4270.

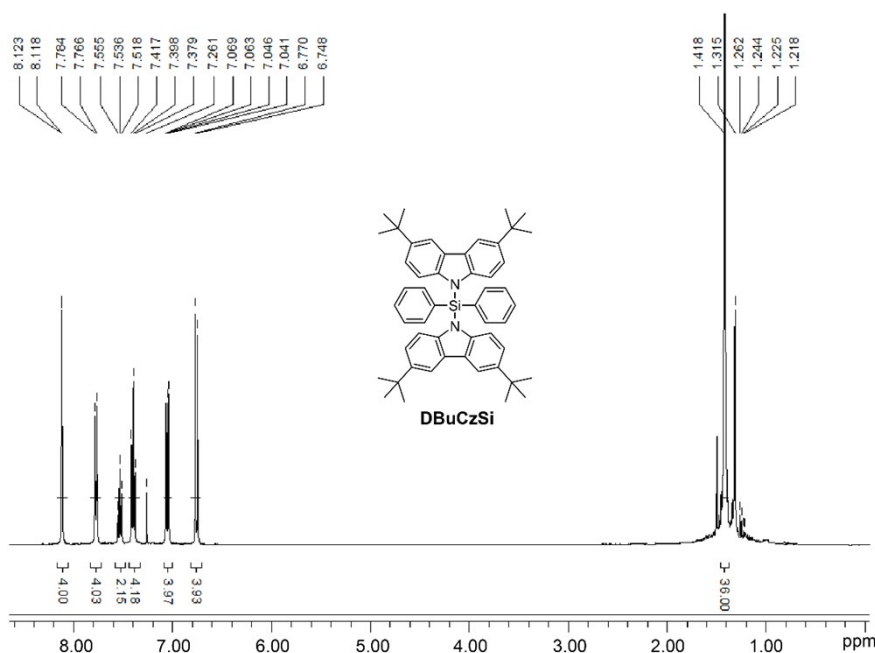


Figure S10. ¹H NMR spectrum of bis(3,6-di-*tert*-butyl-9H-carbazol-9-yl)diphenylsilane (**DBuCzSi**).

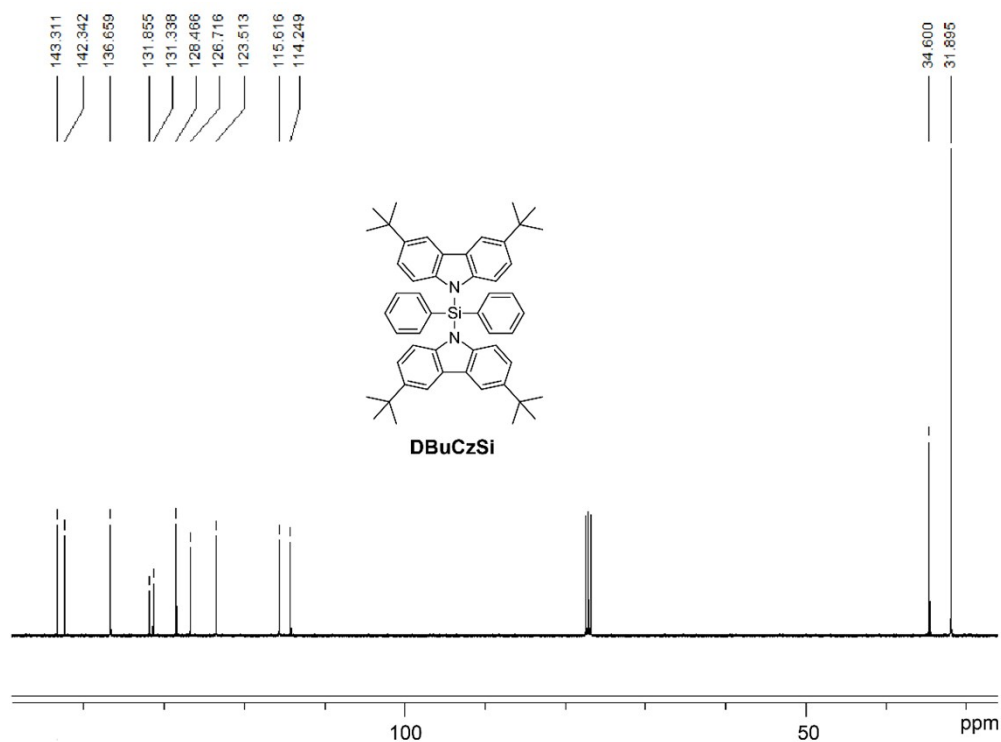


Figure S11. ^{13}C NMR spectrum of bis(3,6-di-*tert*-butyl-9H-carbazol-9-yl)diphenylsilane (**DBuCzSi**).

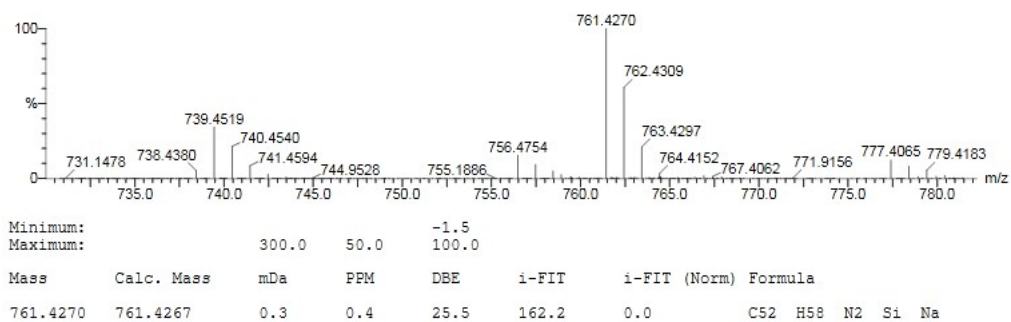


Figure S12. HRMS spectrum of bis(3,6-di-*tert*-butyl-9H-carbazol-9-yl)diphenylsilane (**DBuCzSi**).

2. Single crystal analysis

Single crystals were grown by slow evaporation of a combined CH_2Cl_2 and ethanol solution at room temperature. X-ray crystallography was carried out on a Bruker SMART APEX-II CCD diffractometer with graphite monochromated Mo-K α radiation at 296 K. The crystal structures were analyzed by Diamond 3.2 software and the structure data were summarized in Table S1. The CIF files of the single crystals were also attached.

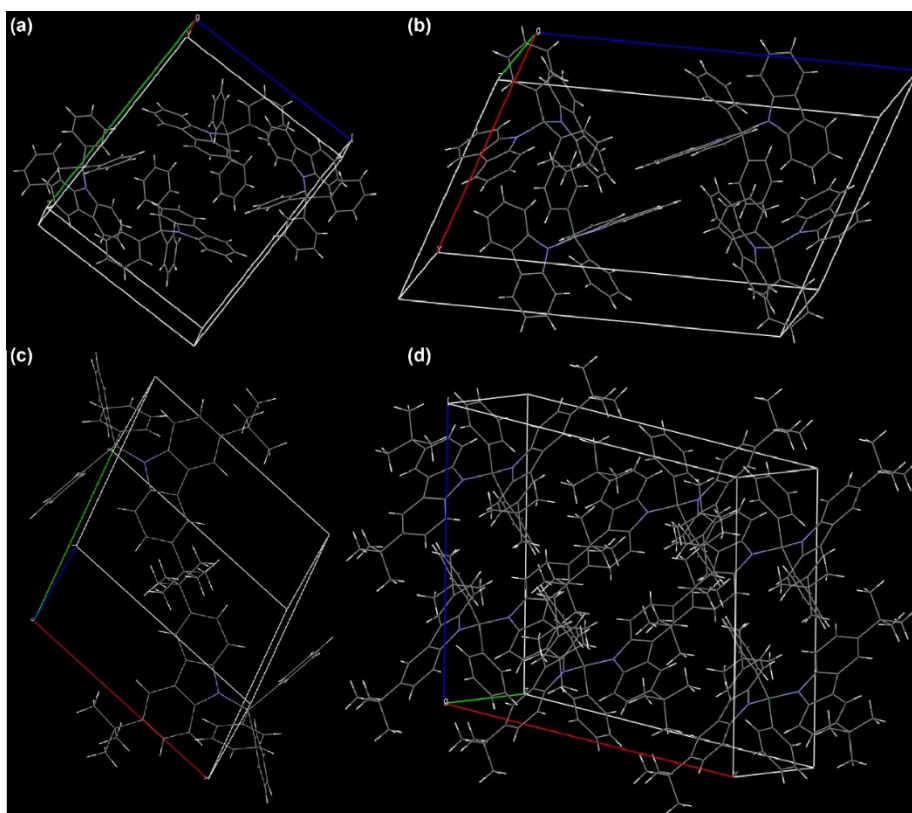


Figure S13. Molecular packing structures in (a) **CzSi**, (b) **DCzSi**, (c) **BuCzSi** and (d) **DBuCzSi** single crystals as revealed by X-ray crystallographic analysis.

Table S1. Crystallographic data of **CzSi**, **DCzSi**, **BuCzSi** and **DBuCzSi**.

Compound	CzSi	DCzSi	BuCzSi	DBuCzSi
Empirical formula	C ₃₀ H ₂₃ NSi	C ₃₆ H ₂₆ N ₂ Si	C ₃₈ H ₃₉ NSi	C ₅₂ H ₅₈ N ₂ Si
Formula weight (g mol⁻¹)	425.58	514.68	537.79	739.09
Crystal color	colorless	colorless	colorless	colorless
Wavelength (Å)	0.71073	0.71073	0.71073	0.71073
Crystal system	monoclinic	monoclinic	triclinic	monoclinic
a, (Å)	9.6528(10)	14.382(4)	11.684(3)	16.008(3)
b, (Å)	16.9821(17)	9.215(2)	11.696(3)	18.367(4)
c, (Å)	13.8598(13)	21.897(5)	12.506(3)	15.659(3)
α, (deg)	90	90	90	90
β, (deg)	91.648(4)	111.629(14)	96.921(3)	102.900(3)
γ, (deg)	90	90	90	90
volume, (Å³)	2271.0(4)	2697.7(11)	1564.3(6)	4488.0(17)
Z	4	4	2	4
Density, (g cm⁻³)	1.245	1.267	1.142	1.094
μ, (mm⁻¹)	0.121	0.116	0.101	0.088
T_{min}, T_{max}	0.983, 0.986	0.983, 0.985	0.986, 0.988	0.988, 0.990
F(000)	896.0	1080.0	1 576.0	1592.0
h_{max}, k_{max}, l_{max}	11, 20, 17	17, 10, 26	11, 11, 12	19, 22, 18
Theta_{max}	26.000	25.000	20.250	25.540

3. Features of N-Si bond

Bond lengths of the N-Si bonds in **CzSi**, **DCzSi**, **BuCzSi** and **DBuCzSi** were achieved from both the single crystal structures and density functional theory (DFT) calculations. The molecular geometries were optimized using the widely used Beckes' three-parameter exchange functional along with the Lee Yang Parr's correlation functional (B3LYP) at 6-31G(d) basis sets. Fuzzy bond order analysis embedded in Multiwfn was used to study the bond order based on the optimized molecular structures at ground state (S_0). Natural bond orbital (NBO) analysis at HF/6-31G(d) level was performed on Gaussian 09 with NBO 6.0 to study the *d*-orbital participation of Si in the N-Si bond based on single crystal structures. The localized orbital locator (LOL) was obtained by employing the Multiwfn version 3.3 software.

Table S2. The bond length, bond order, and Si *d*-orbital participation extent of N-Si and C-Si in **CzSi**, **DCzSi**, **BuCzSi** and **DBuCzSi**.

Comp.	N-Si			C-Si	
	Bond length (Å) ^a	Bond order ^b	<i>d</i> -orbital (%) ^c	Bond length (Å) ^a	Bond order ^b
CzSi	1.7660/1.7938	1.1314	2.35	1.8713/1.8865	1.0287
				1.8628/1.8886	1.0213
				1.8696/1.8869	1.0302
DCzSi	1.7563/1.7776	1.1457	2.55	1.8636/1.8825	1.0233
	1.7597/1.7851	1.1642	2.67	1.8597/1.8809	1.0282
BuCzSi				1.8638/1.8873	1.0293
	1.7627/1.7908	1.1387	2.35	1.8663/1.8886	1.0213
				1.8620/1.8862	1.0282
DBuCzSi	1.7574/1.7824	1.1436	2.59	1.8696/1.8825	1.0325
	1.7575/1.7824	1.1436	2.59	1.8697/1.8825	1.0325

^a Bond length from single crystal and DFT optimization respectively; ^b Fuzzy bond order ;

^c *d*-orbital participation extent of Si calculated by NBO analysis at HF/6-31G(d) level.

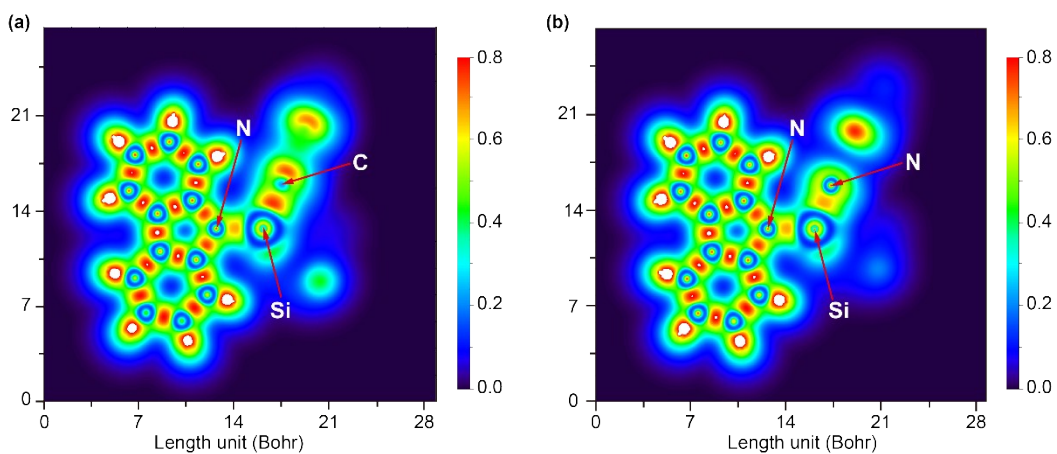


Figure S14. The localized orbital locator (LOL) profiles of (a) **CzSi** and (b) **DCzSi**.

4. Atomic force microscopy

To investigate the film-forming abilities and morphologies of **CzSi**, **DCzSi**, **BuCzSi** and **DBuCzSi** in thin films, atomic force microscopy (AFM) was carried out at room temperature using a Bruker Dimension Icon AFM equipped with Scanasyst-Air peak force tapping mode AFM tips from Bruker.

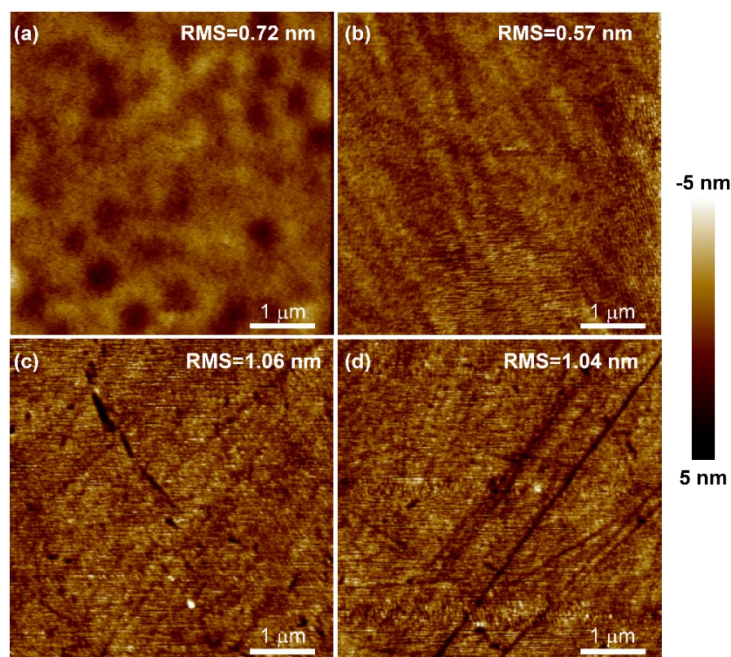


Figure S15. The AFM height images ($5 \times 5 \mu\text{m}^2$) and root-mean-square (RMS) roughness of vacuum-deposited (a) **CzSi**, (b) **DCzSi**, (c) **BuCzSi** and (d) **DBuCzSi** films (100 nm thick) on glass substrates.

5. Thermal properties

Thermogravimetric analysis (TGA) and differential scanning calorimetry (DSC) were performed to investigate the thermal properties of the compounds. TGA measurements were conducted on a Shimadzu DTG-60H thermogravimetric analyses at a heating rate of $10^{\circ}\text{C min}^{-1}$ and a nitrogen flow rate of $50\text{ cm}^3\text{ min}^{-1}$. DSC analyses were performed on a Shimadzu DSC-60A instrument under a heating rate of $10^{\circ}\text{C min}^{-1}$ and a nitrogen flow rate of $20\text{ cm}^3\text{ min}^{-1}$.

6. Optical properties

Ultraviolet-visible (UV-Vis) spectra were recorded on an UV-3600 SHIMADZU UV-VIS-NIR spectrophotometer, while fluorescence spectra were obtained using an RF-5301PC spectrofluorophotometer with a Xenon lamp as light source. The phosphorescence spectra of the compounds in CH_2Cl_2 were measured using a time-resolved Edinburgh LFS920 fluorescence spectrophotometer at 77 K with a 5 ms delay time after the excitation ($\lambda=337\text{ nm}$) using a microsecond flash lamp. The concentrations of the compound solutions (in CH_2Cl_2) were adjusted to be at about $1.0\times 10^{-5}\text{ mol L}^{-1}$. Thin solid films made for optical property measurements were prepared by spin casting solutions of the compounds on quartz substrates.

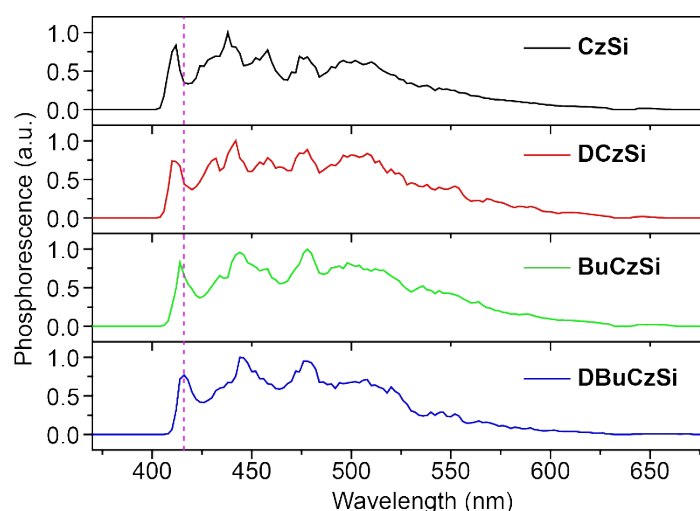


Figure S16. Phosphorescence spectra (excited at 337 nm) of (a) **CzSi**, (b) **DCzSi**, (c) **BuCzSi** and (d) **DBuCzSi** recorded at 77 K in CH_2Cl_2 with a delay time of 5 ms.

7. Electrochemical properties

Cyclic voltammogram (CV) measurements were performed at room temperature to investigate the electrochemical properties of the compounds on a CHI660E system in a typical three-electrode cell with a working electrode (glass carbon), a reference electrode (Ag/Ag⁺, referenced against ferrocene/ferrocenium (FOC)), and a counter electrode (Pt wire) in an acetonitrile solution of tetrabutylammonium hexafluorophosphate (Bu₄NPF₆) (0.1 M) at a sweeping rate of 100 mV s⁻¹. The highest occupied molecular orbital (HOMO) and the lowest unoccupied molecular orbital (LUMO) energy levels (E_{HOMO} and E_{LUMO}) of the materials are estimated based on the reference energy level of ferrocene (4.8 eV below the vacuum) according to the Equations 1 and 2:

$$E_{HOMO} = -[E_{onset}^{Ox} - (0.04)] - 4.8 eV \dots\dots\dots 1$$

$$E_{LUMO} = -[E_{onset}^{Red} - (0.04)] - 4.8 eV \dots\dots\dots 2$$

where the value of 0.04 V is the onset oxidative voltage of FOC vs Ag/Ag⁺ and E_{onset}^{Ox} and E_{onset}^{Red} are the onset potentials of the oxidation and reduction, respectively.

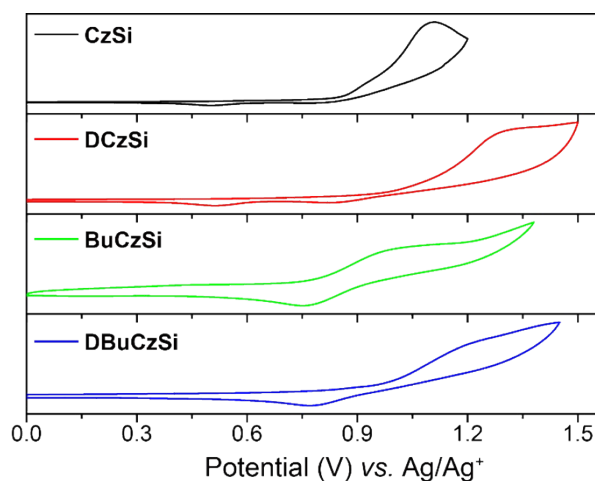


Figure S17. Cyclic voltammograms of CzSi, DCzSi, BuCzSi and DBuCzSi films

Table S3. The optical and electrochemical properties of **CzSi**, **DCzSi**, **BuCzSi** and **DBuCzSi**.

Comp.	T_d^a/T_m (°C)	λ_{abs} (nm)		$^{opt}E_g^b$ (eV)	λ_{em} (nm)		$^{exp}E_T$ (eV)	CV (eV)		Calculation (eV)			
		CH ₂ Cl ₂	Film		CH ₂ Cl ₂	Film		HOMO	LUMO	HOMO	LUMO	$^{cal}E_g$	$^{cal}E_T$
CzSi	295/206	288,315,325	295,317,329	3.69	336,348	335,348	3.02	-5.63	-1.94	-5.36	-0.74	4.62	2.99
DCzSi	329/213	287,310,320	295,316,329	3.68	333,345	333,348	3.02	-5.76	-2.08	-5.51	-0.93	4.58	2.99
BuCzSi	298/257	295,320,330	298,323,334	3.60	345,355	341,356	3.00	-5.56	-1.96	-5.19	-0.72	4.47	2.96
DBuCzSi	359/268	292,317,327	296,318,330	3.63	340,352	338,353	3.00	-5.71	-2.08	-5.30	-0.87	4.43	2.96

^a At 5% weight loss; ^b Estimated from the absorption edge in film.

8. DFT calculations

Theoretical calculations were performed on Gaussian 09 program with the Becke's three-parameter exchange functional along with the Lee Yang Parr's correlation functional (B3LYP) using 6-31G (d) basis sets. The geometries at the ground state (S_0) and the lowest triplet excited state (T_1) were fully optimized by spin-restricted and spin-unrestricted DFT calculations respectively at the B3LYP/6-31G (d) level. The ionization potentials (IPs), hole extraction potentials (HEPs), electronic affinities (EAs), electron extraction potentials (EEPs) and reorganization energies (λ) of these molecules were also calculated to evaluate the energy barrier for injection and transport rates of the holes and electrons when used in optoelectronic devices. The charge (hole and electron) mobility of **CzSi**, **DCzSi**, **BuCzSi** and **DBuCzSi** were assessed using the incoherent hopping model, which assumes a charge transport process between two adjacent reactions $M^\pm + M \rightarrow M + M^\pm$ where M is the neutral molecule interacting with neighboring oxidized or reduced M^\pm .

The hopping rates of charge transfer can be described by the Marcus-Hush equation:

$$K_{h/e} = \frac{V_{h/e}^2}{\hbar} \sqrt{\frac{\pi}{\lambda_{h/e} kT}} \exp\left(-\frac{\lambda_{h/e}}{4kT}\right) \dots\dots\dots 3$$

where $V_{h/e}$ is the electronic coupling matrix element between neighbouring molecules; T is the temperature; k and \hbar refer to the Boltzmann and Planck constants, respectively; $\lambda_{h/e}$ is the hole/electron reorganization energy calculated by the following equations:

$$\begin{aligned} \lambda_h &= \lambda_+ + \lambda_1 \dots\dots\dots 4 \\ \lambda_e &= \lambda_- + \lambda_2 \dots\dots\dots 5 \\ \lambda_+ &= E^+(M) - E^+(M^+) \dots\dots\dots 6 \\ \lambda_1 &= E(M^+) - E(M) \dots\dots\dots 7 \\ \lambda_- &= E^-(M) - E^-(M^-) \dots\dots\dots 8 \\ \lambda_2 &= E(M^-) - E(M) \dots\dots\dots 9 \end{aligned}$$

Table S4. The ionization potential (IP), hole extraction potential (HEP), electronic affinity (EA), electron extraction potential (EEP), relaxation energies (λ_+ , λ_1 , λ_- and λ_2) and reorganization energies (λ_h and λ_e) of **CzSi**, **DCzSi**, **BuCzSi** and **DBuCzSi** calculated by B3LYP/6-31G(d) (in eV).

Comp.	IP	HEP	EA	EEP	λ_+	λ_1	λ_-	λ_2	λ_h	λ_e
CzSi	6.81	6.46	-0.51	-0.19	0.16	0.18	0.14	0.18	0.34	0.32
DCzSi	6.77	6.54	-0.29	0.07	0.14	0.09	0.14	0.22	0.23	0.36
BuCzSi	6.52	6.19	-0.50	-0.07	0.16	0.17	0.17	0.26	0.33	0.43
DBuCzSi	6.37	6.21	-0.29	0.06	0.08	0.08	0.14	0.21	0.16	0.35

9. Charge mobility

In order to experimentally measure the hole and electron mobilities of **CzSi**, **CzSi**, **DCzSi**, **BuCzSi** and **DBuCzSi**, space charge limited current (SCLC) model was applied on hole-only and electron-only devices of ITO/MoO_x (5 nm)/host (100 nm)/MoO_x (5 nm)/Al and ITO/LiF (1 nm)/host (100 nm)/LiF (1 nm)/Al, respectively. The current density (J) in these devices follows the field-dependent space charge limited current (SCLC) model of Mott-Gurney law, which is given as:

$$J_{SCLC} = \frac{9}{8} \varepsilon \varepsilon_0 \mu_0 \exp\left(0.89 \beta \sqrt{\frac{V}{d}}\right) \frac{V^2}{d^3} \dots\dots\dots 10$$

where V is the electrical voltage, d is the film thickness, μ_0 is the average mobility, ε_0 is the permittivity of free space (8.854×10^{-12} F m⁻¹), and ε is the dielectric constant of the film.

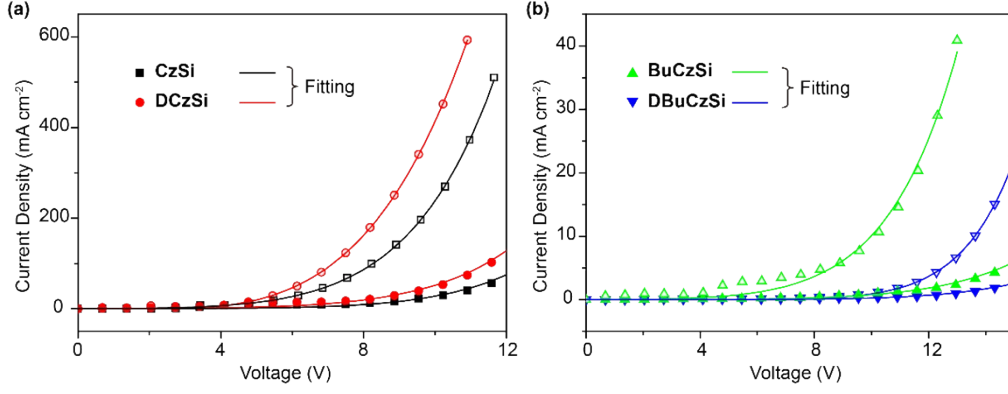


Figure S18. J - V characteristics of (a) CzSi and DCzSi (b) BuCzSi and DBuCzSi-based hole-only and electron-only devices. Symbols show the experimental data, while lines are the fitting curves according to field dependent SCLC model of Equation 11 (closed symbols are for electron-only devices of ITO/MoO_x (10 nm) /host (100 nm)/ MoO_x (10 nm)/Al, while the open symbols for hole-only devices of ITO/LiF (1 nm)/host (100 nm)/ LiF (1 nm)/Al.

10. Device fabrications and measurements

In a general procedure, ITO-coated glass substrates were etched, patterned, and washed with detergent, deionized water, acetone, and ethanol in turn. Organic layers were deposited by high-vacuum ($\approx 4 \times 10^{-4}$ Pa) thermal evaporation at a rate of 0.1–0.2 nm s⁻¹. The layer thickness was measured using Bruker Dektak XT stylus profiler and the deposition rate were monitored *in situ* by an oscillating quartz thickness monitor. The devices without encapsulation were measured immediately after fabrication under ambient conditions at room temperature. Electroluminescent (EL) spectra of the devices were measured by a PR655 spectroscan spectrometer. The luminance-voltage and current-voltage characteristics were recorded using an optical power meter and a Keithley 2400 voltage current source. And the external quantum efficiency (EQE) was achieved by equation 10.

$$EQE = \frac{\pi e \eta_{cd/A} \int \lambda p_{\lambda} d_{\lambda}}{hc K_m \int p_{\lambda} d_{\lambda}} \quad 10$$

where $\eta_{cd/A}$ is the current efficiency (cd A⁻¹); h is the Planck constant; c is the speed of light in vacuum; λ is the wavelength (nm); e is the electron charge; $p(\lambda)$ is the electroluminescent intensity; $\Phi(\lambda)$ is the luminous efficiency; K_m is a constant of 683 lm/W. The lifetime of the blue PhOLEDs

was measured by an M6000 PMX lifetime measurement system in a constant voltage mode.

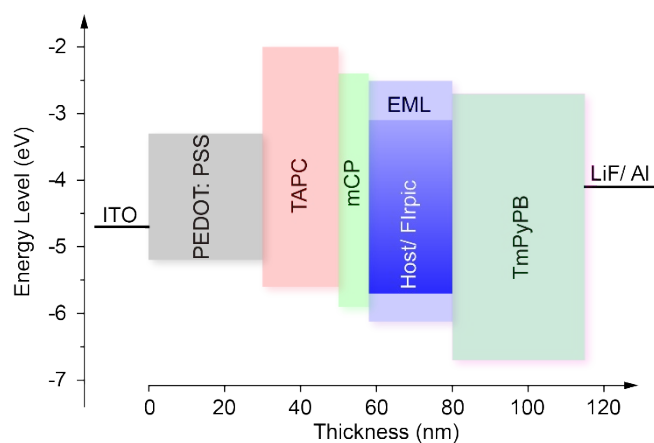


Figure S19. Device configuration and energy diagram of blue PhOLEDs using **CzSi**, **DCzSi**, **BuCzSi** and **DBuCzSi** as the host materials

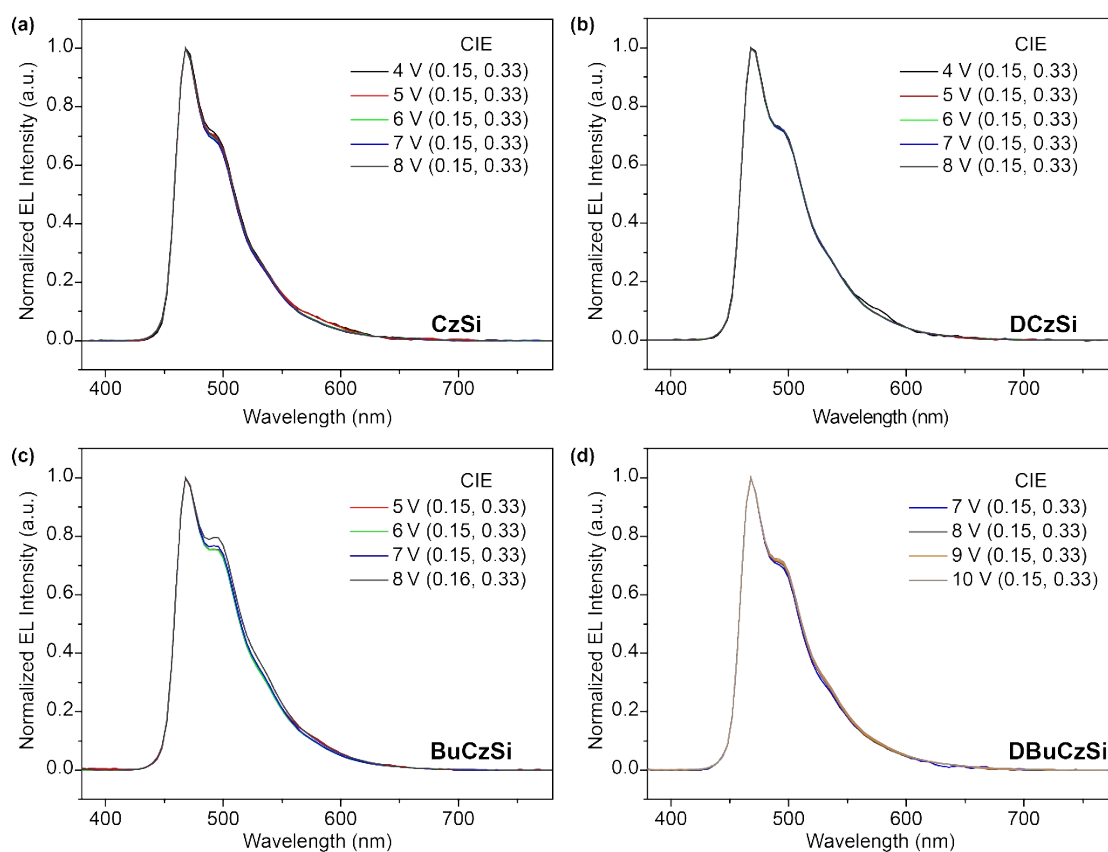


Figure S20. Normalized electroluminescent spectra of the blue PhOLED devices using host materials of (a) **CzSi**, (b) **DCzSi**, (c) **BuCzSi** and (d) **DBuCzSi** at various driving voltages with the corresponding Commission Internationale de l'Eclairage (CIE) coordinates.

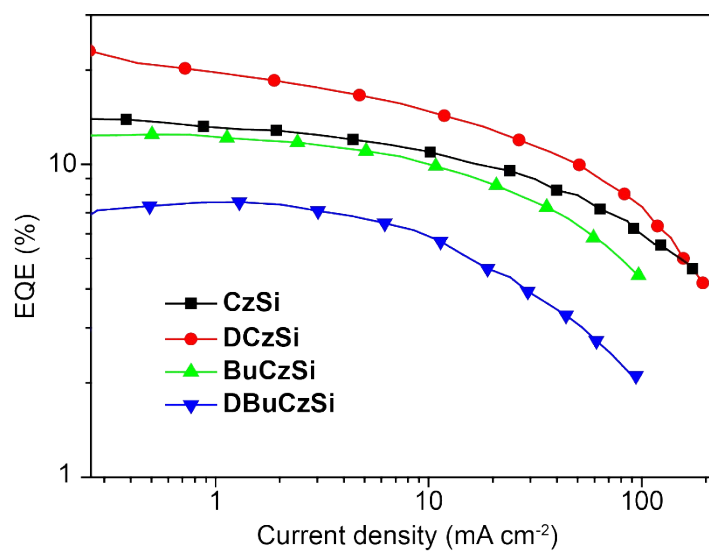


Figure S21. External quantum efficiency (EQE)–current density curves of the PhOLEDs hosted by **CzSi**, **DCzSi**, **BuCzSi** and **DBuCzSi**.

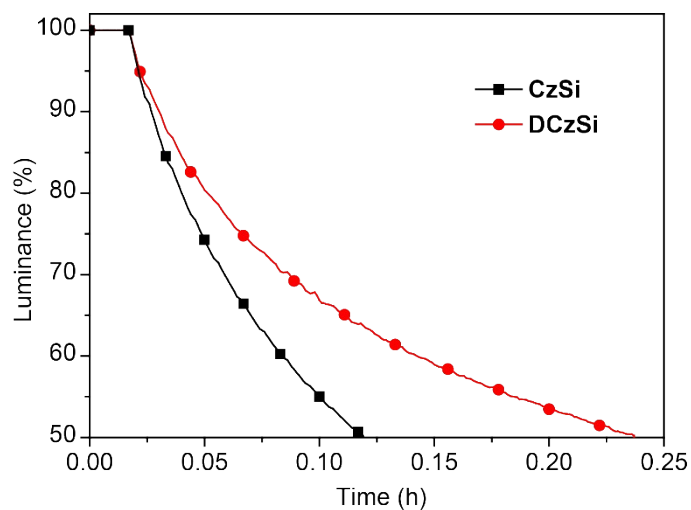


Figure S22. Operation lifetimes of FIrpic-based blue PhOLEDs hosted by **CzSi** and **DCzSi**. The device operation lifetime is measured at an initial luminance of 400 cd/m² in a constant voltage mode.

Table S5. Device performance of the FIrpic-based blue PhOLEDs hosted by **CzSi**, **DCzSi**, **BuCzSi** and **DBuCzSi**.

Comp.	Operating Voltage (V) ^a	Maximum Efficiency ^b	Efficiency ^c			Roll-off ^d			Mobility	
			CE	PE	EQE	CE	PE	EQE	μ_h	μ_e
CzSi	4.6, <7.5, <9.6	23.3, 11.2, 14.0	22.6, 19.3	9.0, 6.1	13.6, 10.9	3.0, 17.5	19.6, 46.4	2.8, 22.1	6.55×10^{-6}	1.13×10^{-7}
DCzSi	3.4, <5.4, <7.2	39.5, 27.4, 24.2	37.6, 30.8	21.7, 13.5	23.1, 17.6	4.8, 22.6	20.8, 50.7	4.5, 27.3	1.80×10^{-5}	1.57×10^{-6}
BuCzSi	6.5, <8.9, <11.0	22.2, 7.9, 12.5	21.2, 19.9	7.6, 5.6	12.4, 11.0	4.5, 10.4	3.8, 29.1	0.8, 12.0	7.33×10^{-7}	3.19×10^{-8}
DBuCzSi	6.5, <8.8, <11.0	13.7, 4.9, 7.6	13.7, 10.4	4.7, 2.9	7.6, 5.7	0.0, 24.1	4.1, 40.8	0.1, 25.0	4.49×10^{-8}	8.44×10^{-9}

^aIn the order of 1, 100 and 1000 cd m⁻²;

^bIn the order of current efficiency (CE, cd A⁻¹), power efficiency (PE, lm W⁻¹) and external quantum efficiency (EQE, %);

^cIn the order of 100 and 1000 cd m⁻²;

^dRoll-off of CE (%), PE (%), and EQE (%) in the order of 100 and 1000 cd m⁻².